Mechanical Systems and Signal Processing 119 (2019) 523–546

Contents lists available at ScienceDirect

Mechanical Systems and Signal Processing

journal homepage: www.elsevier.com/locate/ymssp

Indirect health monitoring of bridges using Mel-frequency cepstral coefficients and principal component analysis

Qipei Mei, Mustafa Gül *, Marcus Boay

Department of Civil and Environmental Engineering, University of Alberta, Edmonton, Alberta T6G 2W2, Canada

ARTICLE INFO

Article history:
Received 23 January 2018
Received in revised form 20 August 2018
Accepted 6 October 2018
Available online 16 October 2018

Keywords:
Structural health monitoring
Vehicle-bridge interaction
Mobile sensor network
Mel-frequency cepstral coefficients
Principal component analysis

ABSTRACT

Bridge health monitoring is a very important part for infrastructure maintenance. Traditional bridge health monitoring techniques require sensors to be installed on bridges, which is costly and time consuming. In order to resolve this issue, new damage detection techniques by installing sensors on passing-by vehicles on bridges and considering vehicle bridge interaction (VBI) have gained much attention from researchers in last decade. In this paper, a novel damage detection technique utilizing data collected from sensors mounted on a large number of passing-by vehicles is developed. First, an approach based on Mel-frequency cepstral coefficients (MFCCs) is introduced. Then, an improved version based on MFCCs and principal component analysis (PCA) taking advantage of mobile sensor network is proposed to overcome the deficiencies in the approaches that utilize single measurement. In the improved approach, the acceleration data is first collected from all the vehicles within a certain period. Then, the transformed features that are related to bridge damage are extracted from MFCCs and PCA. The damage can be identified by comparing the distributions of these transformed features. The results from the numerical analysis and lab experiments show that the approach not only identifies the existence of the damage, but also provides useful information about severity.

1. Introduction

One of the most important components of Structural Health Monitoring (SHM) is detecting damage in existing structures [1,2]. Although this research area only has a relatively short history, it is drawing more and more attention from researchers in structural engineering. By monitoring the structures regularly, the governments can not only avoid loss of lives and wealth due to sudden collapse, but also develop proactive maintenance scheduling to decrease the maintenance and life-cycle costs. Among all the structures, bridges are critical for transportation network, and malfunctioning bridges could cause loss of billions of dollars. In developed countries, most of the bridges were built in 1950s and 1960s. According to Federal Highway Administration (FHWA), nearly 9% of bridges in the United States are structurally deficient [3], and the situation is becoming worse as the bridges approach their design life.

In traditional bridge health monitoring, sensors are installed on bridges, and damage is detected by analyzing the collected vibration data from sensors. This kind of methods has been studied by various researchers over the world [4–9]. However, although these methods provide acceptable accuracy and have the potential to full automation, installation of sensors is expensive and time-consuming. The possibility of bridge closure during installation is also an issue. In fact, a majority

* Corresponding author.
E-mail address: mustafa.gul@ualberta.ca (M. Gül).

https://doi.org/10.1016/j.ymssp.2018.10.006
0888-3270/

of short and medium span bridges do not have structural health monitoring systems due to the difficulties of installing sensors and other practical and economic reasons. To resolve the problems, indirect heath monitoring that is based on vehicle-bridge interaction is taken into consideration. The first paper that utilized this concept to identify bridge information from a passing-by vehicle was written by Yang et al. [10]. In their paper, the equation of motion integrating dynamic properties of both vehicle and bridge was first studied, and then the acceleration of passing-by vehicle was represented as a function of dynamic characteristics of the bridge. After applying Fourier transformation to the vehicle acceleration, the frequencies of the bridge can be identified. Following that, different researchers worldwide did their own work on indirect health monitoring as well [11–20]. Bu et al. [21] proposed an approach based on dynamic response sensitivity analysis using acceleration measurement on the vehicle to identify the damage in the bridge. In their paper, damage, in terms of flexural stiffness reduction, is exposed in an iterative procedure using both 3-parameter and 5-parameter vehicle models. In their numerical analysis, they showed that their approach can detect the damage when measurement noise and road surface roughness exist. Keenahan et al. [15] utilized an instrumented truck-trailer vehicle to monitor the change of damping in a bridge. In their method, the influence of road profile roughness is removed by subtracting one axle acceleration from another, and the change of bridge properties are assessed. In 2012, Zhang et al. [22] proposed an approach to extract Mode Shape Square (MOSS) of the bridge from a passing vehicle with tapping devices that excite the bridge while the vehicle is passing. In their paper, damage feature is defined as the difference of MOSS for intact and damaged bridge. Their numerical analysis and experiments show that the location of damage can be successfully identified even with high level noise. Mcgetrick et al. [23] implemented an experimental validation of a novel passing-by global stiffness identification method. The method proposed in their paper consisted of 6 steps. They first calculated contact force, total displacement and estimated road profile using only acceleration data from the vehicle, and then identified global stiffness of bridge using those variables. In their paper, they found that the method can identify the stiffness correctly for 8 of 9 vehicle-speed combinations, which proves that their method is insensitive to the speed of the vehicle. Matarazzo and Pakzad [24] proposed a method referred as structural identification using expectation maximization (STRIDE) to overcome missing observation issue for modal analysis. They applied this technique to data collected at the Golden Gate Bridge using mobile sensing, and successfully identified 19 modes with high accuracy. Matarazzo and Pakzad [25] also proposed an efficient way called dynamic sensor network (DSN) to store measurement data from a large number of mobile sensing nodes and introduced truncated physical model to process the data. In their paper, two examples, high-resolution mobile sensing and BIGDATA processing, were given to demonstrate the efficiency of DSN. More research about the indirect health monitoring can be found in a comprehensive review written by Malekjafarian et al. [26].

Although promising progresses have been achieved in the area of indirect health monitoring using mobile sensors, there are still challenges that need to be resolved before routine real-life applications [26], such as influence of road profile roughness, limited vehicle-bridge interaction time and environmental effects. In addition, among previous studies, damage can only be detected when the car configurations (natural frequency, speed, etc.) are known or the same car is used for both baseline and damaged cases. In reality, the damage could propagate for years, it is difficult to measure the properties of the car or keep the vehicle's properties the same for every test. Besides, it is costly to have a specifically designed vehicle only for test purpose, and it cannot assess the condition of bridges in real time since the interval of different tests may be very long.

To overcome the issues described above, the authors propose a framework to investigate the potential of employing a large number of mobile sensors (smartphones in vehicles or even embedded sensors in smart vehicles) for indirect monitoring of population of bridges. As shown in Fig. 1, in this framework, data collected from a large number of vehicles passing

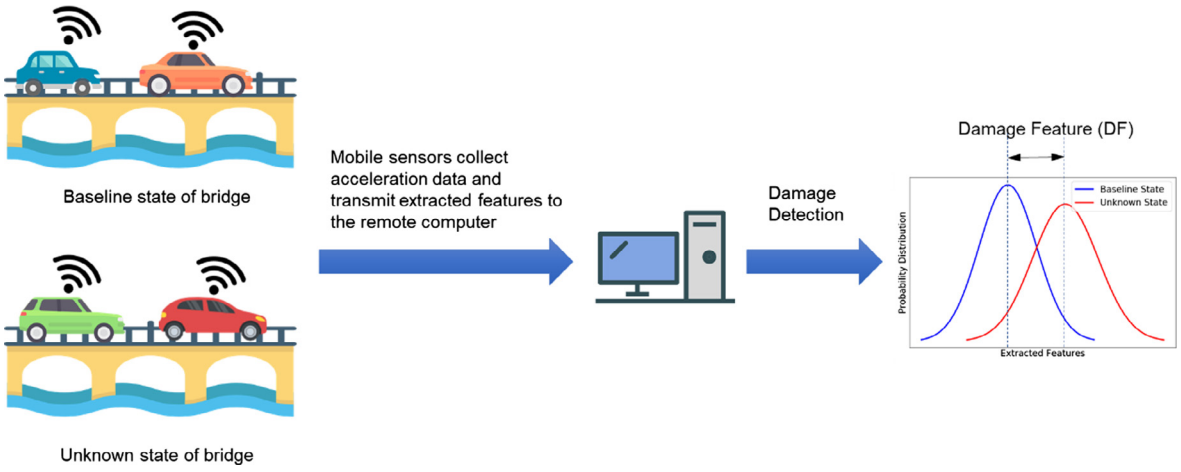

Fig. 1. The framework to utilize a large number of mobile sensors for indirect health monitoring of populations of bridges.

across a bridge within a certain period are used systematically for damage detection. Assuming two cases of the bridge, baseline and unknown cases, the acceleration data from vehicles passing across the bridge within two different periods are collected, and the designed features are extracted from the data before transmitting to the remote computer. Then, the distributions of the extracted features for data collected from two periods are estimated and compared. It should be noted that for the proposed framework, types of vehicles during different periods may be different but they are expected to follow the similar distributions. Since the influence of the types of vehicles is eliminated from the data from a large number of vehicles using proposed data analysis framework, the difference in distributions of extracted features is deemed to be related to the damage in the bridge. Under this framework, populations of bridges can be monitored continuously and simultaneously with the help of a large number of mobile sensors.

Under this framework, a method to extract features based on Mel-frequency cepstrum (MFC) and principal component analysis (PCA) is developed in this paper. This paper consists of two parts.

In the first part, a single-vehicle version of the method based on MFC only is introduced to study the feasibility of using MFC for damage detection using indirect monitoring. Cepstrum is obtained by taking the inverse Fourier transform of the logarithm of spectrum from a signal [27]. It was first developed to study seismic echoes from earthquake and explosions. Currently, the power cepstrum are mainly used to extract characteristics of voice signal. Among various cepstrum-based methods for voice signal processing, MFC is one of the most popular ones. It has been proven as useful in the area of speech recognition [28–30] due to its efficiency and compactness. The main advantages of MFC are that it scans a range of frequencies instead of peak frequencies, and it applies Mel scale instead of Hertz scale to the spectrum to mimic the human auditory system's response. The features extracted by MFC is called Mel frequency cepstral coefficients (MFCCs). In the first part, the Euclidean distance of the MFCCs are used as damage features (DFs).

In the second part, this method is extended to multi-vehicle version with the help of PCA so that data from a large number of vehicles can be used systematically for damage detection. In the improved method, for baseline and unknown cases, the acceleration data of every single vehicle passing through the bridge are collected and processed using MFC. Afterwards, the extracted features are transformed and uncorrelated by PCA. Similar to single-vehicle version, the Euclidean distance of the transformed features are used for damage detection.

2. Part I: Methodology based on adapted MFCCs

2.1. Mel-frequency cepstral coefficients (MFCCs)

In SHM, there are only a few research studies about applying cepstrum for damage detection in recent years, and all of them are applied to non-destructive evaluation or traditional health monitoring using sensors installed on the bridges. In order to detect damage in layered carbon fiber reinforced polymer, Bochud et al. [31] designed a classification system according to cepstral distance to extract features, and applied them in an analysis-by-synthesis scheme for damage detection. Dackermann et al. [32] used cepstrum analysis to generate frequency response functions based on response-only measurements. Then, the difference between baseline frequency response functions and damaged frequency response functions were calculated and passed to PCA to compress the data. At last, neural networks were trained for damage detection. In their paper, the approach was verified both numerically and experimentally.

MFC is a special kind of cepstrum analysis, which has also attracted the interests from researchers of structural health monitoring. Considering that the performance of traditional delamination detection methods is easily affected by environmental noise and subjectivity of the inspector, Zhang et al. [33] introduced independent component analysis to cancel noise, and used MFCCs to remove subjectivity. Then, a radial basis function network was selected for following delamination detection. The experiments and field tests showed that the proposed method had better robustness to noise and still worked even with limited training data. Balsamo et al. [34] proposed an adaption of MFCCs as damage features. Then, the Mahalanobis distance is calculated on those damage features for damage detection. They tested their method first on a numerical 10-DOF shear type system and then a lab structure that behaves nonlinearly. For comparison, damage detection based on auto-regressive coefficients were also conducted as a reference. They concluded that the method based on MFCCs works better than the one based on auto-regressive coefficients. MFCCs has gained more attention recently in the area of SHM, but to the best of the authors' knowledge, there is still no research applying MFCCs to indirect health monitoring for damage detection.

The reason why cepstrum analysis is used for our proposed method is that cepstrum analysis scans and extract information for a range of frequencies instead of just looking for peaks. However, traditional cepstrum analysis assigns equal weights on different frequency ranges while MFC analysis assigns more weights on lower frequency, which is a very important property and more appropriate for bridge monitoring. MFC is originally designed to mimic how human beings respond with their auditory system. For instance, in human auditory system, the conceptual distance between 100 Hz and 200 Hz is much more significant than between 10,000 Hz and 10,100 Hz, even though their linear distances are the same. The situation is similar in bridge frequency domain, the difference in lower frequency range that covers most of the significant modes is usually more significant than the difference in higher frequency ranges. The procedure of MFC is summarized in Fig. 2.

Although MFC is popular for many applications, there is no single Mel-scale formula for the transformation. One of the most widely used formula to transform between linear frequency, f, and Mel-scale frequency, m, is presented in Eqs. (1) and (2) [35]. The transformation using this formula is presented in Fig. 3.

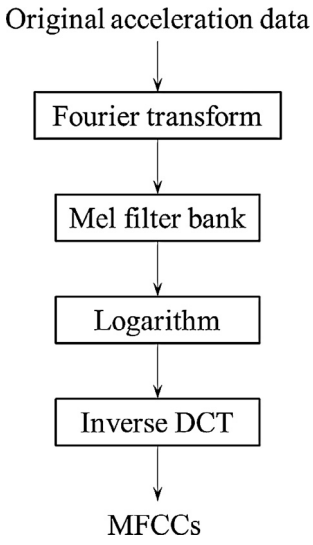

Fig. 2. Procedure of MFC.

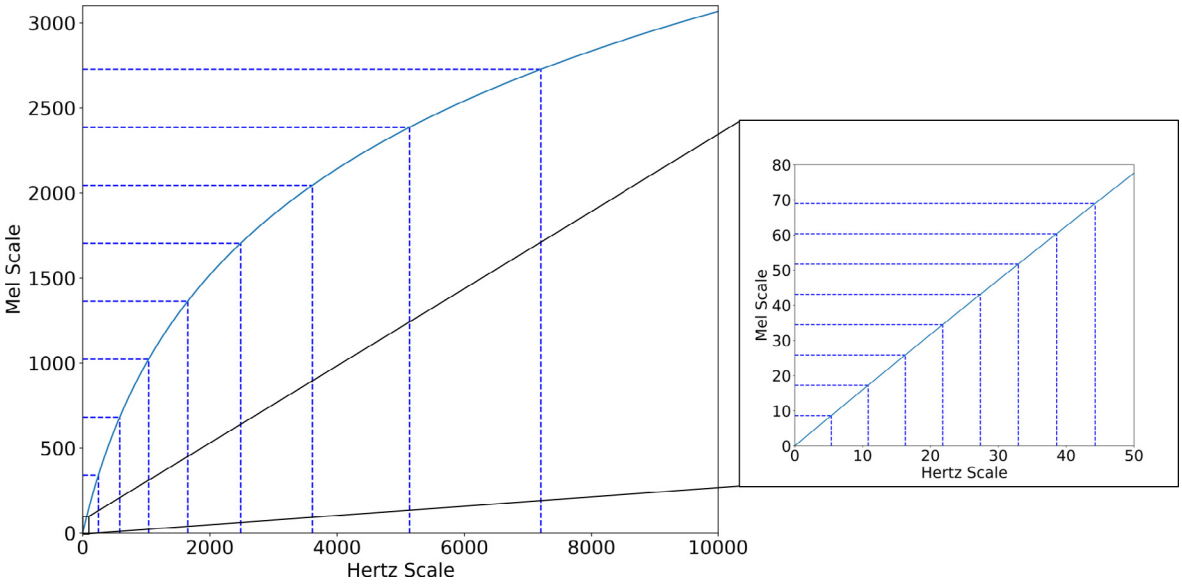

Fig. 3. Transformation between Hertz Scale and Mel Scale.

$$m = M(f) = 1127\ln\left(1 + \frac{f}{700}\right) \tag{1}$$

$$f = M^{-1}(m) = 700\left(e^{m/1127} - 1\right) \tag{2}$$

where f is the Hertz-scale frequency and m is the Mel-scale frequency.

However, the traditional Mel-scale was developed to mimic human auditory system which is most sensitive to frequencies between 2000 and 5000 Hz. This is much higher than the range of natural frequencies in bridges (0–100 Hz). Using this formula, the low frequencies are still linear after the transformation (as shown in Fig. 3).

Therefore, the original Mel scale that was designed for speech signal is not applicable to bridges. Such conclusion was also given in [34]. Considering that lower frequency of bridges is always more important, we propose an adapted formula for the transformation to mimic the trending of Mel-scale in Eqs. (3) and (4). The relationship between adapted Mel scale and Hertz scale is shown in Fig. 4.

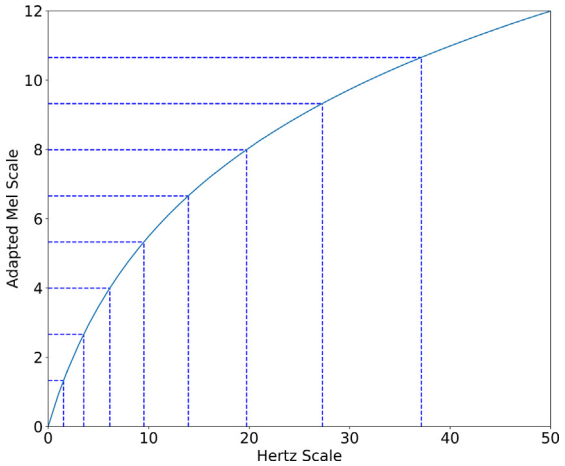

Fig. 4. Transformation between Hertz Scale and Adapted Mel Scale.

$$m = M(f) = 5\ln\left(1 + \frac{f}{5}\right) \tag{3}$$

$$f = M^{-1}(m) = 5\left(e^{m/5} - 1\right) \tag{4}$$

where f is the Hertz-scale frequency and m is the Mel-scale frequency.

Adapted Mel-scale frequency can be linearly separated into n segments. The ith Hertz-scale frequency corresponding to ith adapted Mel-scale frequency is presented in Eq. (5). Generally, larger n leads to smaller triangles in following analysis, which focuses more on details of the power spectrum. However, if n is too large, the obtained MFCCs may not capture the generalization of the spectra and result in poor performance. It is seen in Fig. 4 that linearly separated adapted Mel-scale frequencies correspond to in Hertz-scale frequencies with exponential growing intervals.

$$f_i = M^{-1}\left(M(f_1) + (i-1) \times \frac{M(f_n) - M(f_1)}{n-1}\right) \tag{5}$$

A set of triangular filters called filter bank are applied to the spectrum at each of the Mel-frequency. In speech recognition, the number of triangular filters is usually between 20 and 40. The shape of the filter bank is demonstrated in Fig. 5. The function of the filter bank is represented in Eq. (6):

$$H_i(k) = \begin{cases} 0 & k < f_{i-1} \\ \frac{k - f_{i-1}}{f_i - f_{i-1}} & f_{i-1} \le k < f_i \\ \frac{f_{i+1} - k}{f_{i+1} - f_i} & f_i \le k < f_{i+1} \\ 0 & k \ge f_{i+1} \end{cases}, \quad i = 2, 3, \cdots, n-1 \tag{6}$$

where $H_i(k)$ is the ith filter bank that is applied to the power spectrum.

Since both power spectrum and filter are represented in frequency domain, applying filter to the original signal is to simply multiply the power spectrum by the filter. Then, the summation of the energy after applying all the filters is presented below:

$$E(i) = \sum_k H_i(k) \times F(k), \quad i = 2, 3, \cdots, n-1 \tag{7}$$

where $F(k)$ is the Discrete Fourier Transform (DFT) of the original acceleration signal. Then, the logarithms of the powers are taken at each of the Mel frequencies:

$$\log E(i) = \log\left(\sum_k H_i(k) \times F(k)\right), \quad i = 2, 3, \cdots, n-1 \tag{8}$$

The last step of the cepstrum analysis is to take the Discrete Cosine Transform (DCT) of the logged powers as they are signals.

$$X_j = \sum_{i=2}^{n-1} \log E(i) \cos\left[\frac{\pi}{n-2}\left(i - \frac{3}{2}\right)j\right], \quad j = 1, 2, 3, \ldots, n-2 \tag{9}$$

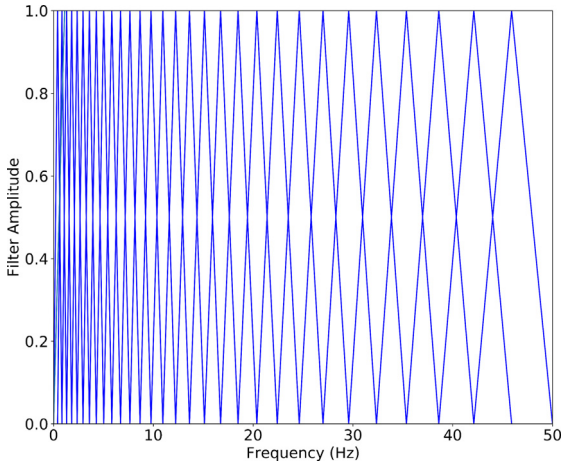

Fig. 5. Filter bank for frequency ranging from 0 to 50 Hz.

where X_j is denoted as Mel-frequency cepstral coefficients or MFCCs. Usually, not all MFCCs are used as inputs for further analysis.

For damage detection, the Euclidean distance of the MFCCs are used as damage features (DFs):

$$\mathrm{DF} = \sqrt{\sum_{j=n_1}^{n_2} \left(X_{j0} - X_{jk}\right)^2} \tag{10}$$

in which X_{j0} stands for jth MFCC for baseline case and X_{jk} stands for jth MFCC for unknown case k (e.g. damaged case). Only MFCCs ranging from n_1 and n_2 are utilized in the DF calculation. According to our analysis, the first four coefficients are more related to the global vibration of the damage and not very sensitive to the damage, and therefore features 4–9 (6 features) are utilized for DF calculation.

2.2. Numerical simulation

In order to verify the above-mentioned approach, first numerical analysis for a single span beam-type bridge is conducted in Abaqus. The bridge is made of steel, and is 2000 mm long, 304 mm wide and 12.7 mm thick. As shown in Fig. 6, a spring mass model is introduced to simulate the vehicle passing over the bridge. The bridge itself is meshed into 16 elements as presented in Fig. 7. The mass of the vehicle is set to 3 kg, and the spring constant of the spring is 266.7 N/m. Using the configuration, the natural frequency of the vehicle is 1.5 Hz. The speed of the car is set to 1 m/s.

Except baseline case, 7 damage cases are introduced. DC1 to DC3 are related to stiffness reduction of elements 7 and 8 (mid-span), DC4 to DC6 are created by changing stiffness of elements 4 and 5 (1/4 span), and DC7 is about boundary condition changes at both ends. The stiffness changes for DC1-DC6 are simulated by reducing elastic modulus. To simulate the measurement error, all damage cases are corrupted with 5% artificial noise. Except baseline case and 7 damage cases, a validation case is introduced with the same setup as baseline but different noise and referred as DC0. The validation case and eight damage cases are summarized as below:

Fig. 6. Spring mass vehicle bridge interaction model (adapted from [10]).

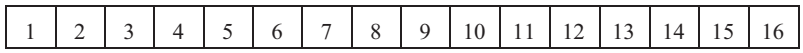

Fig. 7. Mesh grid of the bridge.

1) DC0: No damage (validation case)
2) DC1: 10% reduction of stiffness at mid-span
3) DC2: 20% reduction of stiffness at mid-span
4) DC3: 30% reduction of stiffness at mid-span
5) DC4: 10% reduction of stiffness at ¼ span
6) DC5: 20% reduction of stiffness at ¼ span
7) DC6: 30% reduction of stiffness at ¼ span
8) DC7: Both ends are changed to fixed supports.

2.3. Results and analysis

2.3.1. DC1-DC3: Stiffness reduction at mid-span

For DC1 to DC3, the numerical simulation for each damage case is repeated 20 times with noise added. From Fig. 8, it is seen that the existence of stiffness reduction can be identified accurately with DFs derived from MFCCs. The DFs from validation case are close to zero even though 5% noise is added to the data. 10% stiffness reduction at mid-span leads to DFs of around 2. As the damage becomes more severe, the magnitude of the DFs increases accordingly. For different trials, the DFs fluctuate within an acceptable range, which means the DFs can distinguish real damage from noise.

2.3.2. DC4-DC6: Stiffness reduction at ¼ span

Similar to DC1 to DC3, DC4 to DC6 introduce stiffness reduction, but now at the ¼ span instead of mid-span. From Fig. 9, we can see that the DFs shows the existence of damage very well with high robustness. In addition, the values of DFs are also related to the severity of damage. When comparing Figs. 8 and 9, it is seen that at the same percentage of stiffness reduction, the DFs for mid-span cases are larger to ¼ span cases. From our modal analysis, the first natural frequency of the bridge drops from 7.3365 Hz to 7.0047 Hz if the damage occurs at mid-span, but for ¼ span damage, the first frequency only drops to 7.1755 Hz. We can see that damage at mid-span has larger impact on the overall performance of the bridge.

2.3.3. DC7: Boundary condition changes

Fig. 10 illustrates the most severe damage case introduced in the simulation, change of boundary conditions at both ends. We can see from the figure that the DFs for this case is around 11, which is almost twice as DFs for 30% stiffness reduction at mid-span and thrice as DFs for 30% stiffness reduction at ¼ span. This concludes that the DFs derived from MFCCs are sensitive to not only the existence but also the severity of the damage.

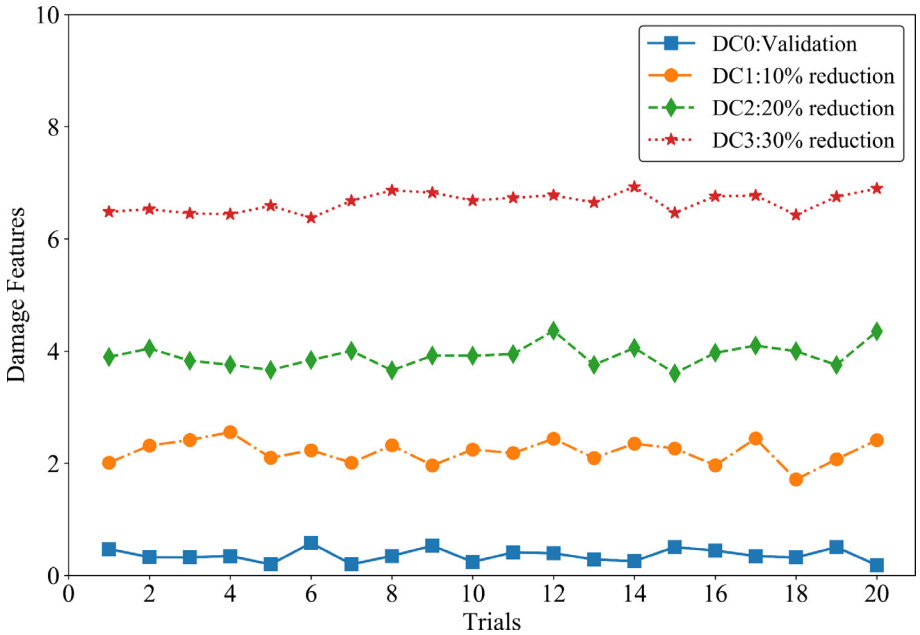

Fig. 8. DFs for DC1-DC3 (single vehicle).

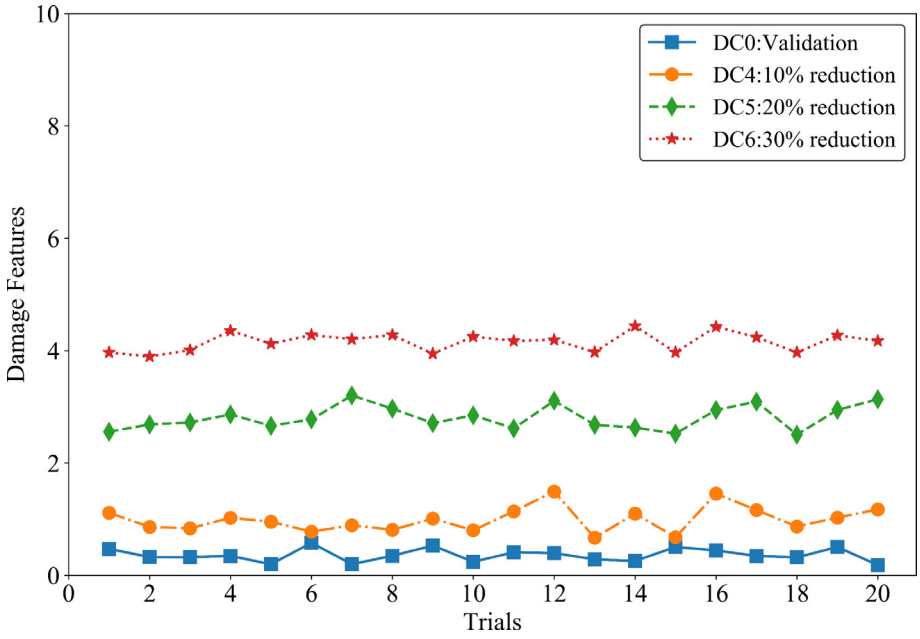

Fig. 9. DFs for DC4-DC6 (single vehicle).

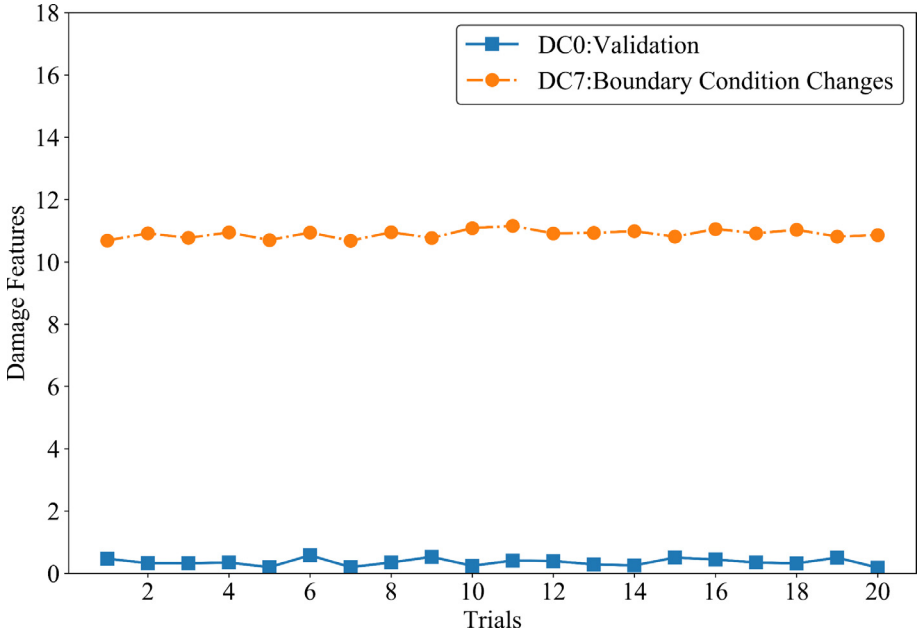

Fig. 10. DFs for DC7 (single vehicle).

3. Part II: An improved methodology taking advantage of a large number of vehicles

3.1. Mobile sensor network

In last section, MFCCs have been proven sensitive to damage and robust to the noise. However, in such damage detection approach, the parameters of the vehicles, such as natural frequency or speed, must be kept the same or very similar for different tests so that the variation of vehicle configurations would not mask the real damage on bridge. Also, the tests have to be scheduled on a single bridge at a time in order to detect damage.

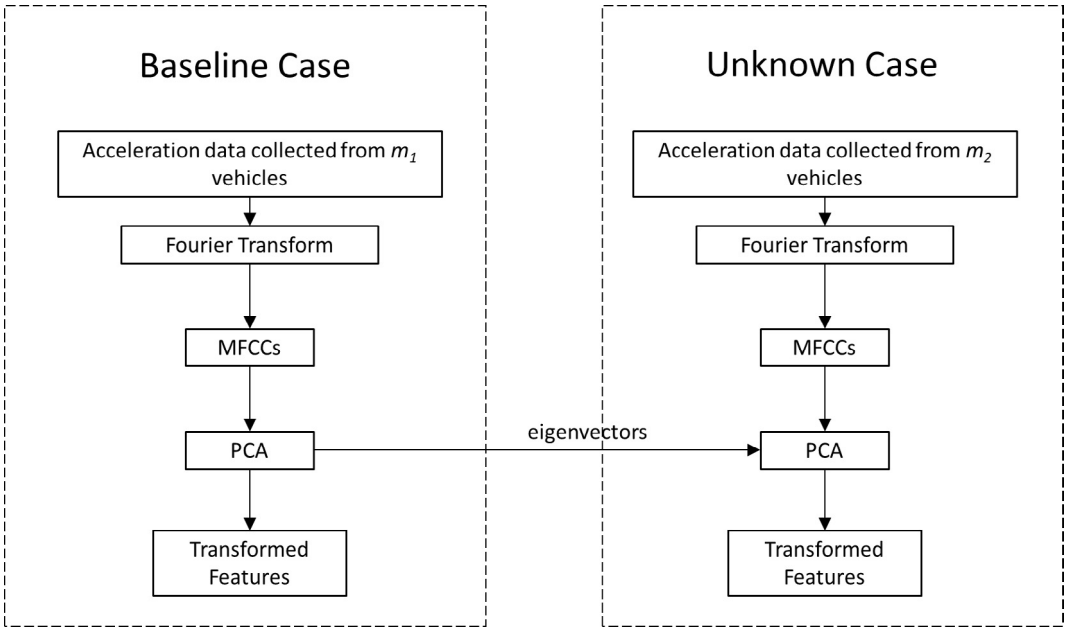

Fig. 11. Procedure to obtain transformed features.

In recent years, Internet of Things technologies have been developing significantly [36,37]. Sensors can easily be installed on smart devices, such as electric vehicles and cell phones, and they usually have the ability to connect to Internet. Therefore, large amount of data (i.e. 'big data') can be collected in real time for analysis use [38,39]. In this section, an improved methodology is proposed for damage detection of bridges by conducting a PCA based statistical analysis of the MFCCs extracted from data collected from large number of drive-by vehicles. Using this approach, although the type of vehicles may vary for different tests, the statistical characteristics of all the vehicles can be used for damage detection. Under the framework of mobile sensor network, the monitoring process could be distributed over a population of bridges and be real time with the help of several thousands or tens of thousands of vehicles, if not more.

3.2. Principal component analysis

Unlike MFC, PCA has been applied for SHM extensively for years [40–42]. Zang and Imregun [43] used PCA as a pre-process step for frequency response functions based damage detection. Using the frequency response functions with reduced dimensionality as input, artificial neural network provides good performance for damage detection. Tibaduiza et al. [44] proposed an approach that integrates a multiactuator system, PCA and self-organizing maps, and experimentally showed that their approach can successfully classify baseline cases and six damage cases. Park et al. [45] invented an approach based on PCA and k-means. In their approach, an on-board active sensor system was utilized to collect impedance data. PCA was applied to eliminate unwanted noise in impedance data, and then k-means unsupervised learning algorithm was employed for damage detection. The approach was verified through a bolt-jointed aluminum structure with loosing bolts.

In other studies, PCA is usually used for dimensionality reduction. In our approach, after the MFCCs are extracted, PCA is used to transform them into a space that the features are uncorrelated so that each transformed feature can be compared separately. Assuming we get q features from MFC, the original features are stored in a matrix called $\mathbf{X_k}$, and $X_{ij,k}$ represents the jth feature for ith vehicle for damage case k. The first step of PCA is to subtract the column-wise mean from each row:

$$X'_{ij,k} = X_{ij,k} - \frac{1}{m}\sum_{i=1}^{m} X_{ij,k}, \quad j = 1, 2, 3, \cdots, q \tag{11}$$

where m is the number of vehicles for each damage case, and q is the number of features we extracted from MFC.

Then, the covariance matrix can be derived as below,

$$\boldsymbol{C_k} = \begin{bmatrix} \mathrm{cov}(X'_{1,k}, X'_{1,k}) & \mathrm{cov}(X'_{1,k}, X'_{2,k}) & \cdots & \mathrm{cov}(X'_{1,k}, X'_{q,k}) \\ \mathrm{cov}(X'_{2,k}, X'_{n_1,k}) & \mathrm{cov}(X'_{2,k}, X'_{2,k}) & & \mathrm{cov}(X'_{2,k}, X'_{q,k}) \\ \vdots & & \ddots & \vdots \\ \mathrm{cov}(X'_{q,k}, X'_{q,k}) & \mathrm{cov}(X'_{q,k}, X'_{2,k}) & \cdots & \mathrm{cov}(X'_{q,k}, X'_{q,k}) \end{bmatrix} \tag{12}$$

$$\mathrm{COV}\left(X'_{u,k}, X'_{v,k}\right) = \frac{1}{m-1}\sum_{i=1}^{m} X'_{iu,k}X'_{iv,k} \quad u, v = 1, 2, 3, \cdots, q \tag{13}$$

The covariance matrix is q by q. The eigen-values and eigen-vectors of the covariance matrix must satisfy the following equation:

$$\boldsymbol{C_k} \times \boldsymbol{V_k} = \boldsymbol{\lambda_k} \times \boldsymbol{V_k} \tag{14}$$

where $\mathbf{V}$ is the eigen-vector matrix and λ is the eigen-value matrix. The transformation of features is implemented by multiplying original features by eigen-vectors [46].

$$\boldsymbol{Y_k} = \boldsymbol{X_k} \times \boldsymbol{V_k} \tag{15}$$

where $\mathbf{Y_k}$ is the transformed feature matrix, in which $Y_{ij,k}$ is the jth transformed feature for ith vehicle in damage case k.

3.3. Damage detection procedure

The procedure to obtain the transformed features is summarized in Fig. 11. For the baseline case of the bridge, acceleration data from m_1 passing-by vehicles are collected within a certain period of time. MFCCs are calculated using the data from every single vehicle. Then, PCA is implemented for all m_1 vehicles passing across the bridge at baseline case. In this way, the average of each transformed feature is set to zero since PCA normalizes the data. For the unknown case, acceleration data from m_2 passing-by vehicles are collected within another period of time. MFCCs are calculated for the unknown case and then, the MFCCs are transformed using the eigenvectors obtained by the PCA conducted with the baseline case data. In this way, the transformed features for the data from both baseline and unknown cases can be compared in the same space.

Following the above procedure, each vehicle has q transformed features. When a large volume of acceleration data are collected, each transformed feature would have m_1 samples for baseline case and m_2 samples for unknown case where m_1 and m_2 are the number of vehicles for both baseline and unknown cases. Although the numbers of samples for each transformed feature are different for baseline and unknown cases, the statistical characteristics are still comparable assuming the types of vehicles follow the similar distributions. The damage detection procedure using transformed features is described in Fig. 12.

The damage detection procedure in this section is based on the premise that if the bridge is damaged, the statistical characteristics of the transformed features should vary when the distributions of vehicle configurations are similar. In this paper, the Euclidean distance of the mean of the distributions of all transformed features for baseline and unknown cases are considered as an indicator of damage, i.e. Damage Feature (DF). The DFs are calculated as below:

$$\mathrm{DF} = \sqrt{\sum_{j=1}^{q}\left(\frac{1}{m_1}\sum_{i=1}^{m_1} Y_{ij,0} - \frac{1}{m_2}\sum_{i=1}^{m_2} Y_{ij,k}\right)^2} \tag{16}$$

where $Y_{ij,0}$ is the jth transformed feature of ith vehicle for baseline case, and $Y_{ij,k}$ is the jth transformed feature for ith vehicle in unknown case k.

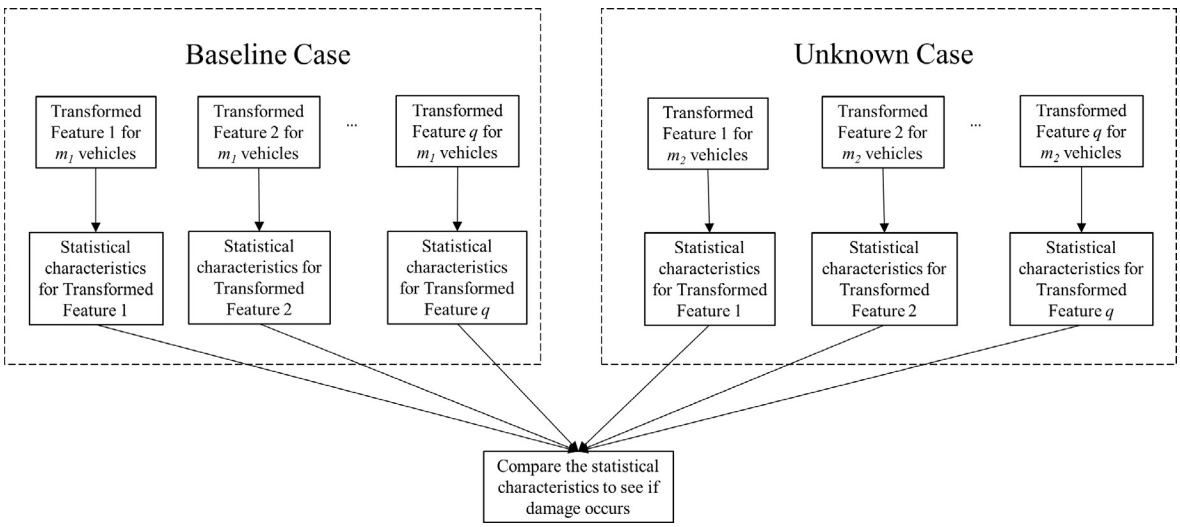

Fig. 12. Procedure to detect damage.

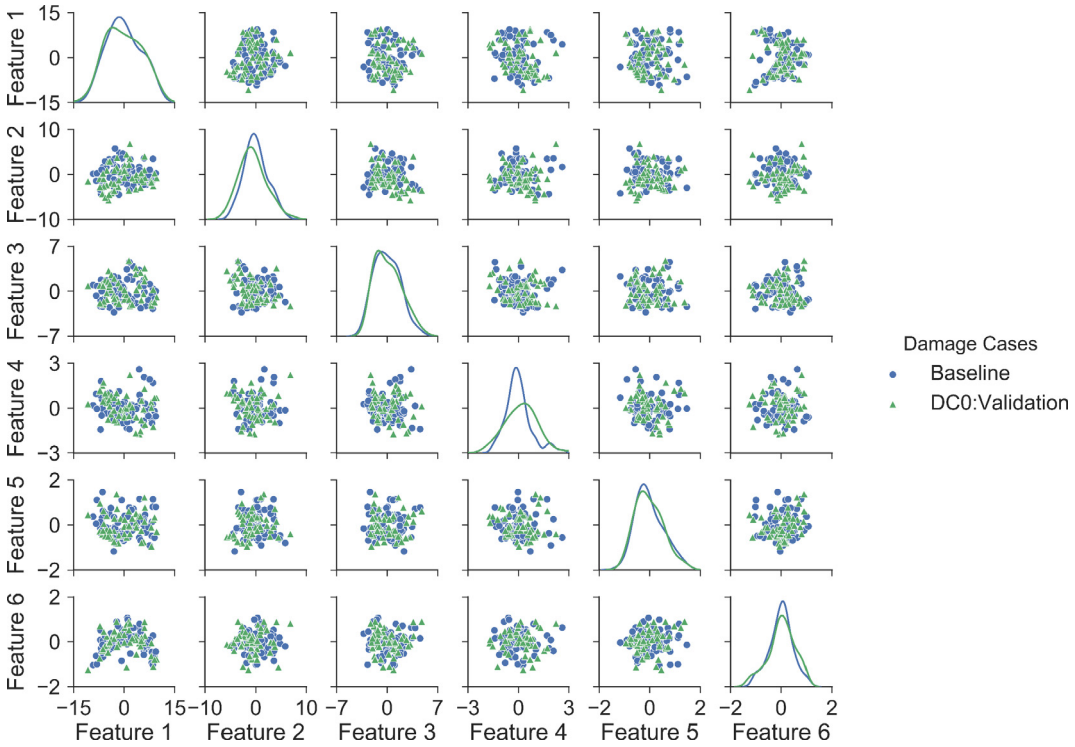

Fig. 13. Pairwise plots of transformed features for baseline and validation cases (multiple vehicles).

3.4. Numerical verification

In this section, numerical setup which is the same as the one in Section 2 is used. Since the method proposed in this part requires a large number of tests, the parameters are changed in spring mass model to simulate different vehicles. To be specific, for each damage case, the following changes are made for the vehicle:

a) The spring constant of the vehicle is changed to 50%, 75%, 100%, 125%, and 150% of its original value
b) The mass of the vehicle is changed to 50%, 75%, 100%, 125%, and 150% of its original value
c) The speed of the vehicle is changed to 50%, 75%, 100%, 125%, and 150% of its original value

Therefore, there are $5 \times 5 \times 5 = 125$ tests for each bridge configuration. For the healthy state of the bridge, we randomly pick 60% of the tests ($60\% \times 125 = 75$) and reserved them for baseline case. The remaining 40% healthy data are used for validation ($40\% \times 125 = 50$). All damaged cases with 125 data entries are compared with baseline case built with 75 randomly picked data entries. In this way, we can verify the approach even when the distributions of the car configurations are not exactly the same for baseline and unknown cases. The whole process is repeated 10 times. In each time, different data entries in baseline case are picked.

3.5. Distribution of transformed features

The distributions of all 6 transformed features for baseline and validation cases calculated by the approach proposed in this part are shown in Figs. 13 and 14. In Fig. 13, the diagonal plots demonstrate the probability density curves of transformed features in baseline and validation cases. For instance, the plot at the first row and the first column represents the probability density curves of transformed feature 1. It is seen that the curves for all transformed features are very close to each other even though they have different number of samples and configurations for vehicles. Since the transformed features are distributed in 6 dimensional space (6 transformed features), pairwise plots for any of two transformed features are given in order to visualize the patterns better. The off-diagonal pairwise scatter plots show that the transformed features vary even when no damage exists. The probabilistic approach proposed in our study provides a tool to identify whether the change is caused by the real damage or just the variation of vehicle configurations. If only the approach in part I is utilized, there will be a big chance to obtain false positive or negative results due to changes in vehicle configurations. In contrast, it is reasonable to compare statistical characteristics of two clusters constructed by a number of data points. In this way, the impact of variation of vehicle configurations or noise from single measurement can be significantly reduced.

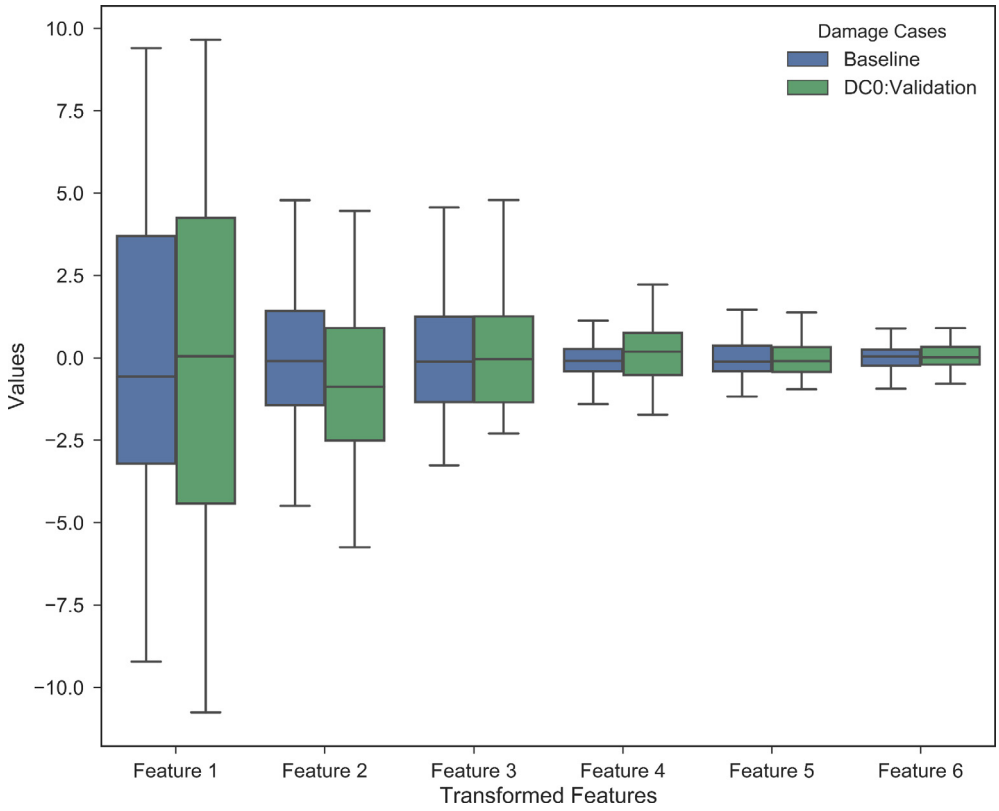

Fig. 14. Boxplot of transformed features for baseline and validation cases (multiple vehicles).

Fig. 14 shows the boxplot of all 6 transformed features as another way to represent the distributions. In such plot, the band inside the box represents the median of the transformed feature, while the top and bottom of the box indicates the first and third quartiles. The maximum and minimum values of each transformed feature are also marked on the boxplot. Using boxplot, we can see the distributions of all 6 transformed features for baseline and validation cases are indeed very similar.

3.6. Results and analysis

3.6.1. DC1-DC3: Stiffness reduction at mid-span

The results for cases of stiffness reduction at mid-span are shown in Figs. 15–17. The probability density curves and pairwise relationships of all 6 transformed features for baseline case, DC1 and DC3 are presented in Fig. 15. The blue circles represent the features for baseline case, while green triangles and red squares are for DC1 and DC3, respectively. In the off-diagonal plots of Fig. 15, it is seen that the transformed features for each case tend to form a cluster. In other words, when the vehicle configurations change, the transformed features tend to vary around a center. The center of the cluster moves when the state of the bridge changes. In the plots, it is seen that the center of the transformed features for DC3 has larger shift from the baseline than the center from of the transformed features for DC1, which is a sign that the center of the clusters can be used as an indicator for relative severity assessment. Also from the pairwise scatter plots, since the points with different colors have some overlaps with each other, which indicates that changes in those transformed features caused by the variation of vehicle configurations, such as frequency and speed, may be at the same level as those caused by damage. Therefore, it is deemed that employing the MFC approach proposed in part I using single vehicle measurement may not reliable when the vehicle changes, because the change of transformed features caused by the variation of vehicle configuration could mask the ones caused by the damage in bridge. When looking at the probability density curves in Fig. 15 and box plots in Fig. 16 of those transformed features for various vehicles, it is also seen the deviation has become larger as the damage becomes more severe. This demonstrates that the statistical characteristics of the transformed features using MFC and PCA are more reliable for indirect health monitoring of bridges using data collected from a large number of vehicles.

The DFs calculated from transformed features are presented in Fig. 17. They are grouped by damage cases, and each group includes ten trials (with different artificial noise and sampling). Compared with the validation case, the DFs for DC1 to DC3 are larger. For 10% stiffness reduction at mid-span, the DFs are around 1.5, while the DFs are about 5 for 30% stiffness reduction cases. The DFs gradually increase as the damage become more severe, which means that the improved approach can still

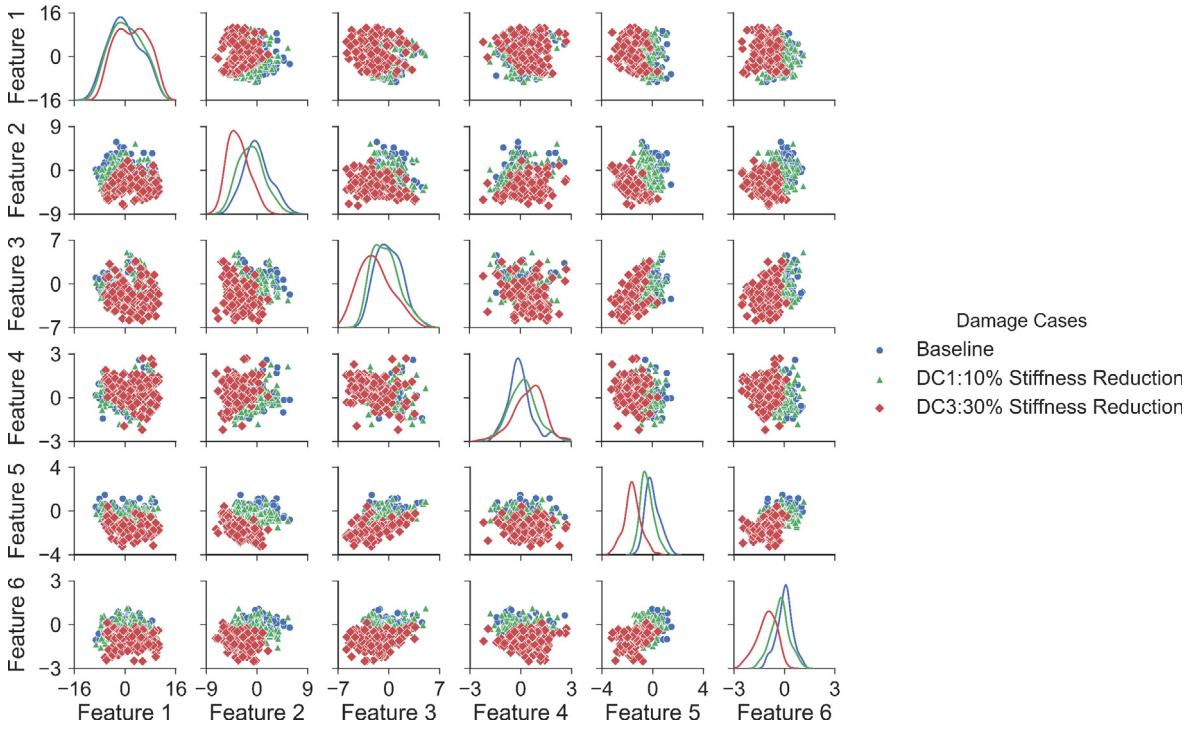

Fig. 15. Pairwise plots of transformed features for baseline case, DC1 and DC3 (multiple vehicles).

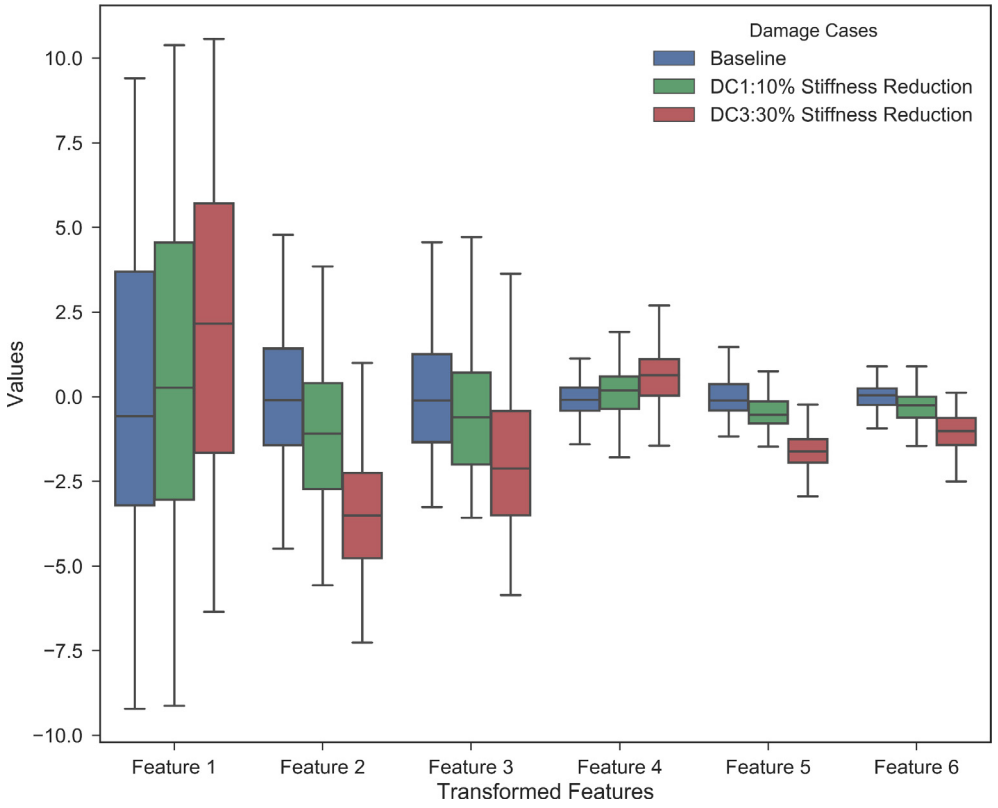

Fig. 16. Boxplot of transformed features for baseline case, DC1 and DC3 (multiple vehicles).

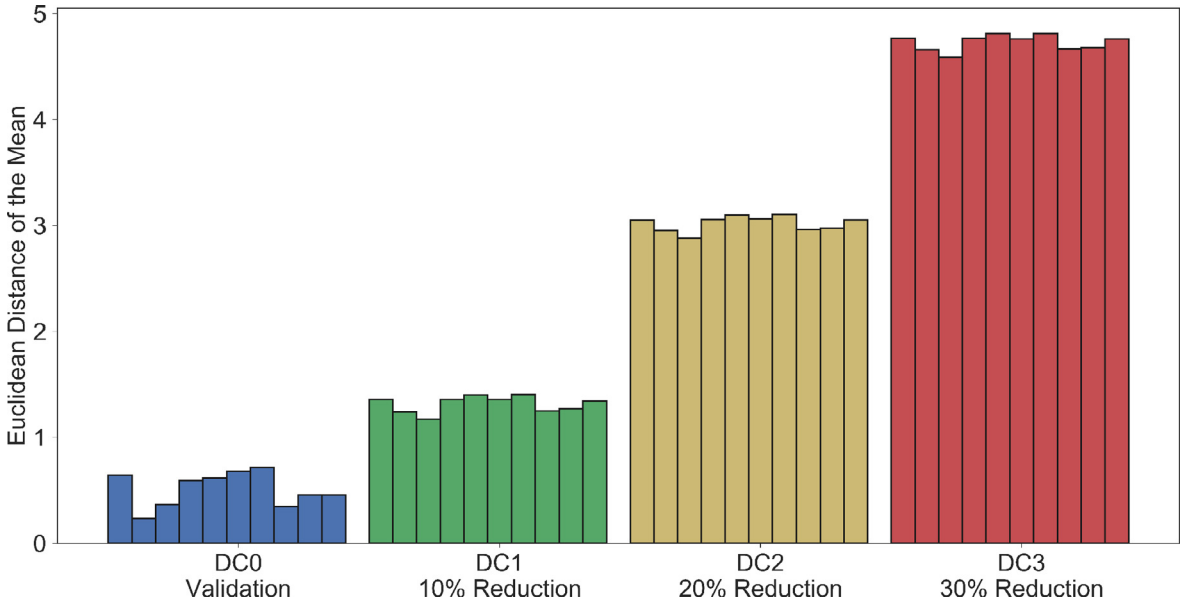

Fig. 17. DFs for validation case, DC1, DC2 and DC3 (multiple vehicles).

show the existence and severity of the damage without any issues. In addition, for 10 trials within each damage case with added artificial noise, the DFs values are very stable, which shows that the DFs are robust to randomness in sampling process.

3.6.2. DC4-DC6: Stiffness reduction at ¼ span

In Figs. 18 and 19, the distributions of transformed features related to stiffness reduction at ¼ span are demonstrated. It is shown that the patterns for transformed features in DC4 to DC6 are very similar to patterns in DC1 to DC3 since they are all damage caused by stiffness loss. Like in DC1-DC3, the centers of the clusters for DC4 to DC6 are still related to the state of the bridge. In Fig. 19, it is seen that as damage increases, transformed features 1, 2, 3 and 5 decrease, and transformed features 4 and 5 increase. In the multi-dimensional transformed feature space, we are measuring the absolute shift of cluster centers for damage detection, and the direction of deviation should not affect the results. Therefore, Euclidean distance is used to define the DFs.

As mentioned above, the DFs derived from transformed features as Euclidean distance of the mean values are presented in Fig. 20. In this figure, we can still see that the DFs are higher as the damage increases. Comparing Figs. 17 and 20, we can see that DFs for mid-span cases is larger than for ¼ cases when the same percentage of stiffness loss is applied. This is because that stiffness loss at mid-span has more impact on the global performance of the bridge.

3.6.3. DC7: Boundary condition changes

DC7, boundary condition changes at both ends, is very severe damage compared to other local damage simulated. The pairwise scatter plots and probability density curves for 6 transformed features are presented in Fig. 21. From both scatter points and probability density curves, we can tell that the difference of the distributions of transformed features between baseline and DC7 is much larger than other cases. From Fig. 22, it is seen that the means of all 6 features deviate from baseline significantly. Like all other damage cases, the DFs derived from Euclidean distance of thetransformed features are presented in Fig. 23. The DFs for DC7 are around 9 for this case, which is almost twice as DFs for 30% stiffness reduction at mid-span in Fig. 17. The DFs are also stable among 10 trials with different sampling and artificial noise.

3.6.4. Influence of number of vehicles

In the previous analysis, 75 vehicles are randomly selected for baseline case, while 125 vehicles are used for other cases. As discussed in previous sections, the DFs fluctuate because different sets of vehicles are used for baseline and other cases. The artificial noise added to the acceleration data could also lead to fluctuation. In this section, the influence of the number of vehicles on the DFs is investigated. In Fig. 24, the coefficient of variance (CoV) of DFs is plotted against 25–100 vehicles for baseline case. It is seen that the CoV of DFs is higher when a small number of vehicles are used for baseline case. The reason is that when the data set is not big enough, the estimate of distribution is not as accurate. When the number of vehicles increases, the CoV for DFs decreases gradually. Therefore, it is safe to say that the method is more robust when larger number of vehicles are used which is very promising for real-life applications with big-data extracted from large number of vehicles.

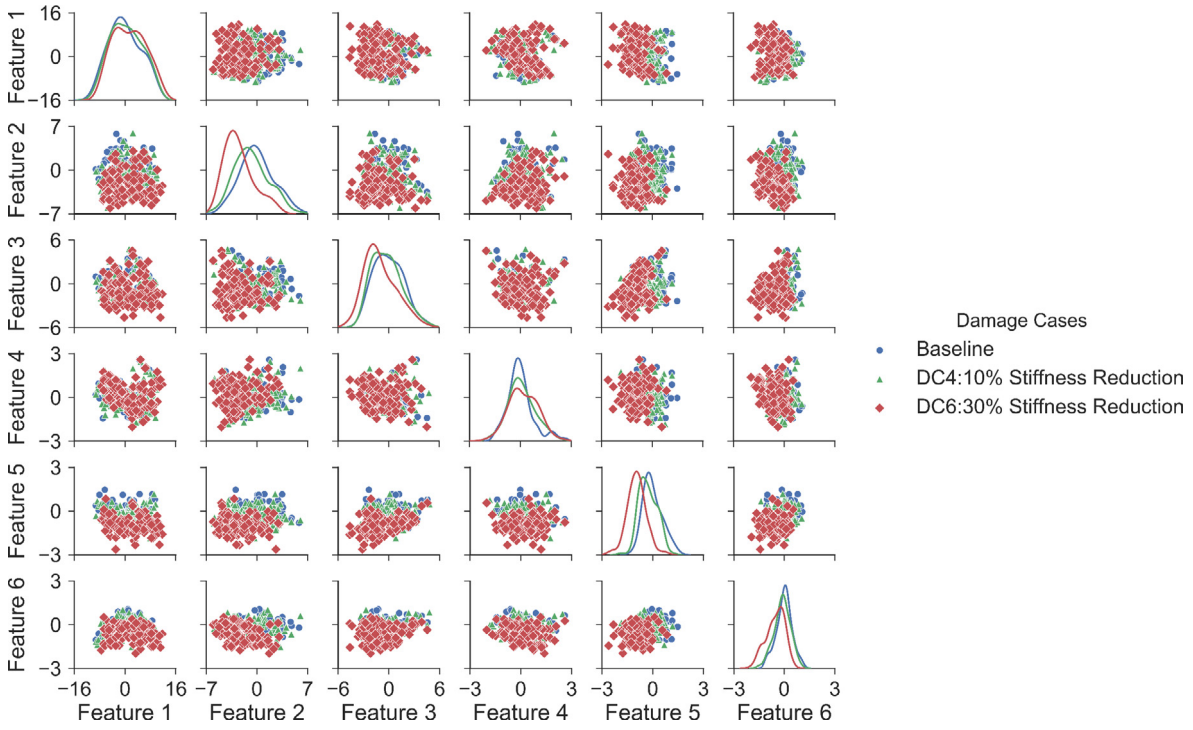

Fig. 18. Pairwise plots of transformed features for baseline case, DC4 and DC6 (multiple vehicles).

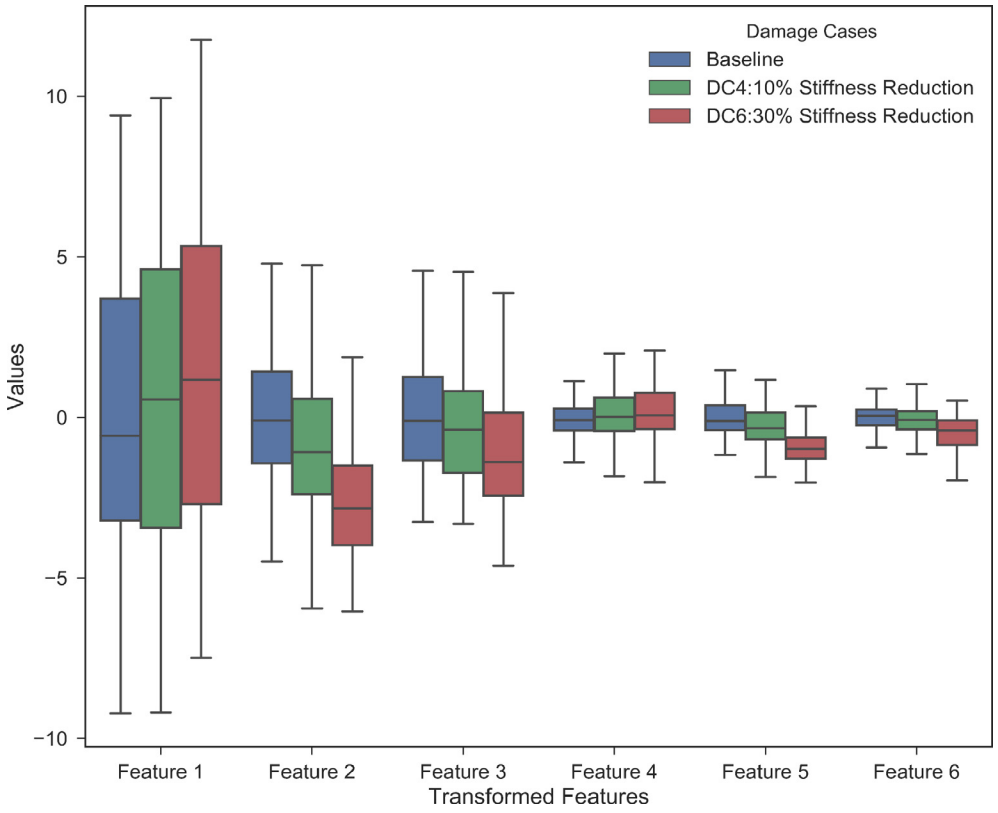

Fig. 19. Boxplot of transformed features for baseline case, DC4 and DC6 (multiple vehicles).

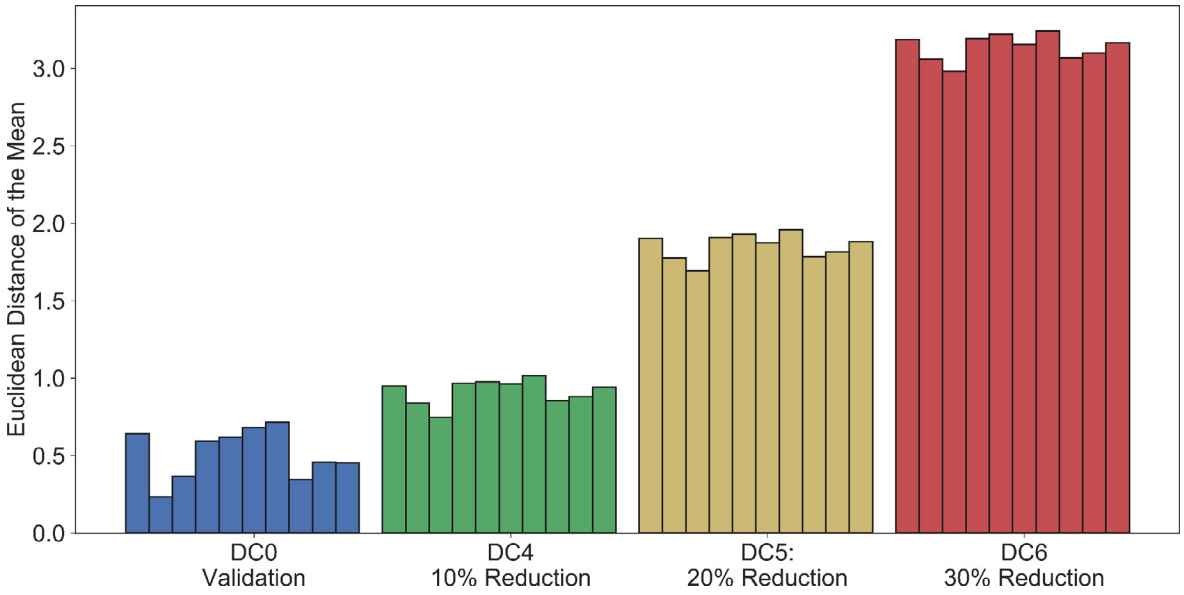

Fig. 20. DFs for DC4-DC6 (multiple vehicles).

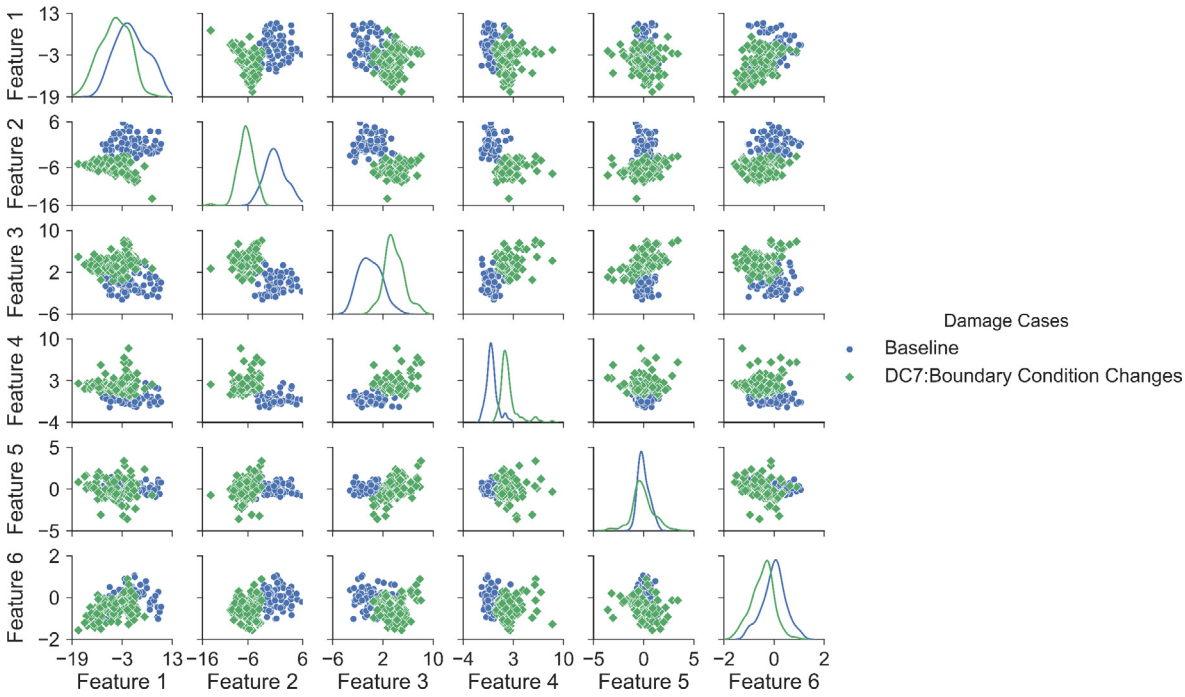

Fig. 21. Pairwise plots of transformed features for baseline case and DC7 (multiple vehicles).

3.6.5. Influence of number of transformed features

In previous analysis, 6 transformed features calculated through MFC and PCA are used for damage detection. In order to investigate the effect of number of transformed features on the performance of the method, the number of features is changed between 4 and 10 and a sensitivity analysis is conducted. The ratio of the average DF between damaged cases and DC0 are used as an indicator to show the distinguishability of the DF. As can be seen in Fig. 25, the changes in the ratios for DC1-DC6 as the number of transformed features increase are negligible. The performance of DF is considered quite stable for different number of transformed features. Therefore, in practice, this parameter is not expected to have a significant impact on the results.

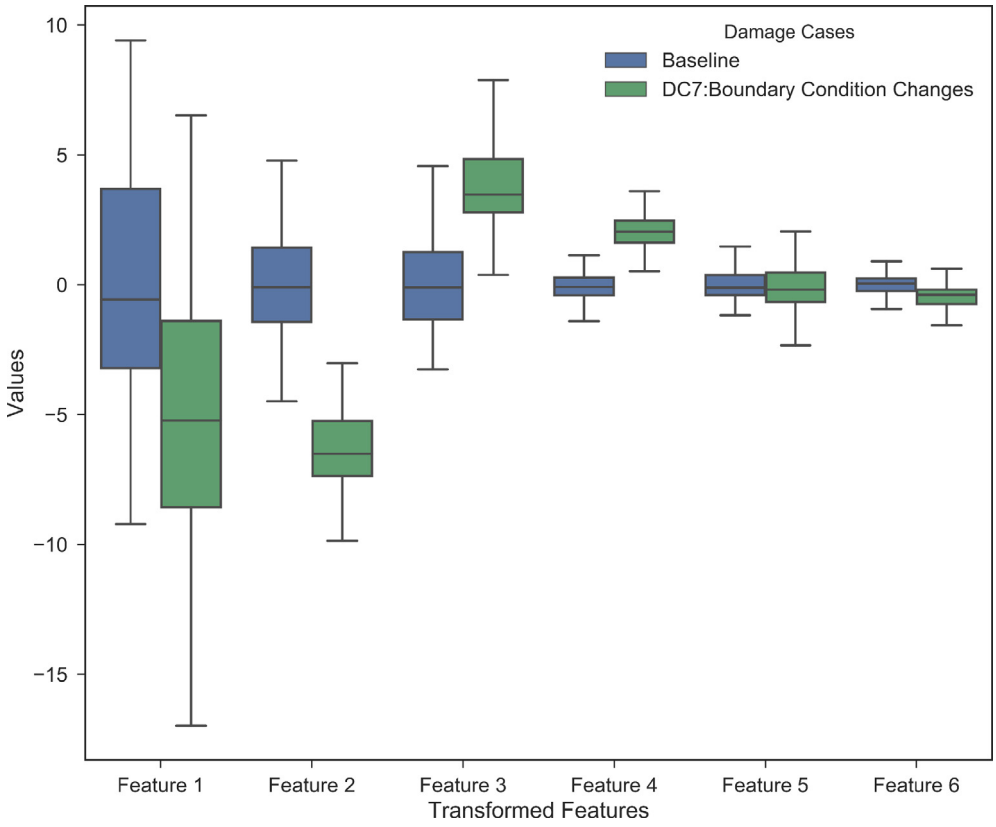

Fig. 22. Boxplot of transformed features for baseline case and DC7 (multiple vehicles).

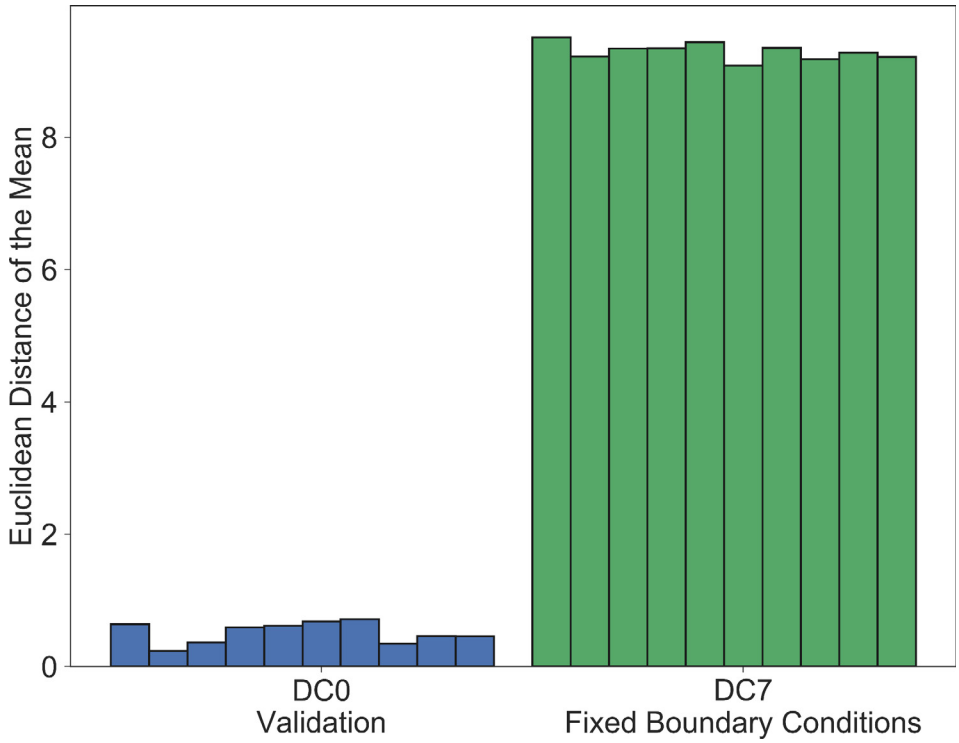

Fig. 23. DFs for DC7 (multiple vehicles).

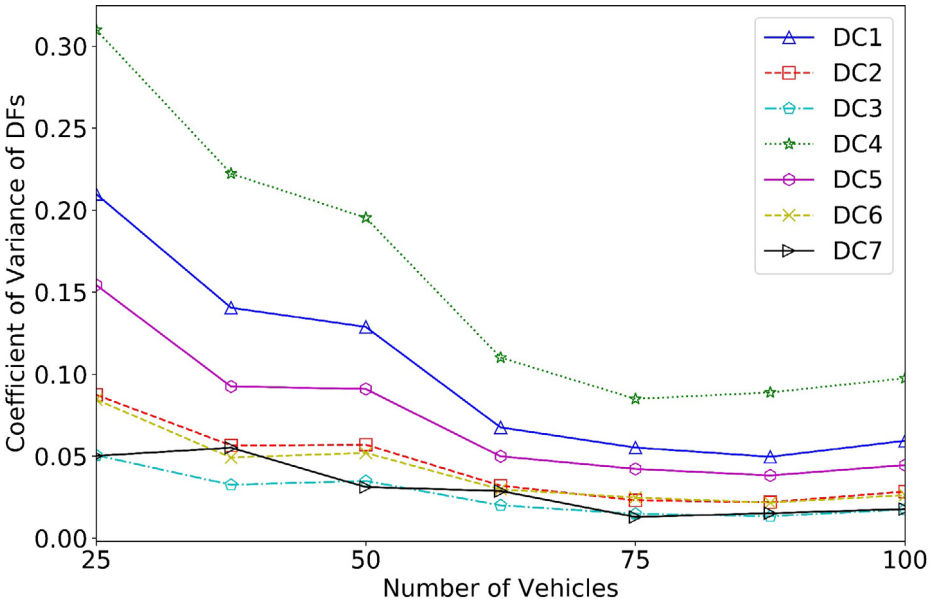

Fig. 24. Relationship between CoV of DFs and number of vehicles.

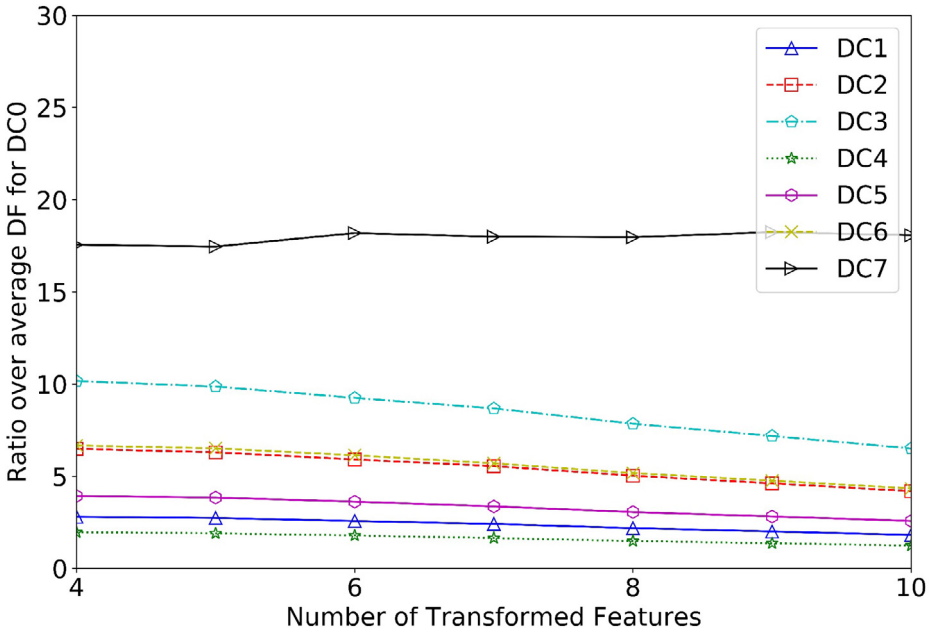

Fig. 25. Ratio over average DF of DC0 for different number of transformed features.

4. Experimental verification

4.1. Experimental setup

In addition to numerical simulations, lab experiments are conducted to verify the improved approach proposed in part II (see Fig. 26). In the experiments, a simply supported bridge is used. The bridge deck is made of steel. The length of the bridge is 2000 mm, the width is 304 mm and the thickness is 12.7 mm.

A robot car is designed to simulate the spring mass vehicle in terms of frequency. The sensors and added masses are mounted on the top plate of the car, and the data acquisition system is installed on the chassis of the car. To simulate

Fig. 26. Setup of the lab experiment.

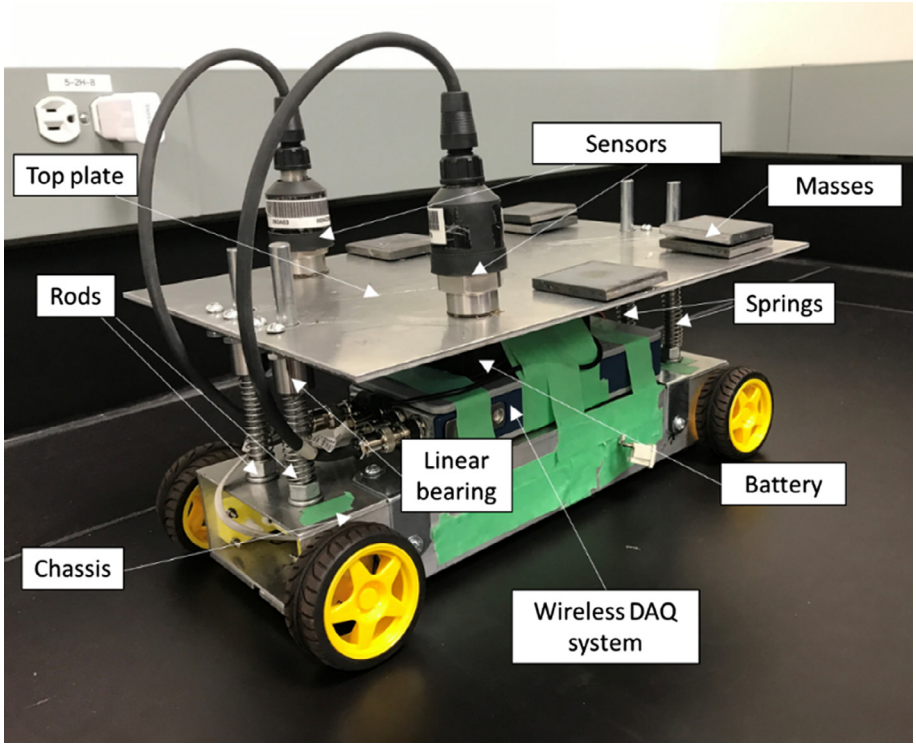

Fig. 27. Components of the robot car.

the suspension system, four rods with springs are installed on the car. The top plate is connected to the chassis of the car through linear bearings. The chassis of the car is 2.710 kg. The configuration of the robot car is demonstrated in Fig. 27. It is powered by 5 AA batteries and controlled by Arduino UNO board, which are mounted inside the chassis of the car. The vertical acceleration is measured through two PCB 393A03 accelerometers and a NI9234 DAQ system with sampling frequency of 1652 Hz. NI LabVIEW is the software for data acquisition.

Similar to numerical analysis in Section 3, the configuration of the vehicle is changed to simulate the variety of vehicles passing across the bridge. The change in the properties of three components, i.e. weights of the top plate, speed of the car, and spring constants of the suspension system, are considered in the experiments, since these three parameters could affect the dynamic behavior of the vehicles significantly. As shown in Table 1, for each component, three values are used. The weight of the top plate is changed by putting additional mass on the middle of the top plate. The speed is changed by adjust-

Table 1
Variation of car components.

	1	2	3
Weights of top plate (kg)	2.094	2.350	2.604
Speed (m/s)	0.09	0.185	0.250
Spring Constants (N/m)	368.4	420	580

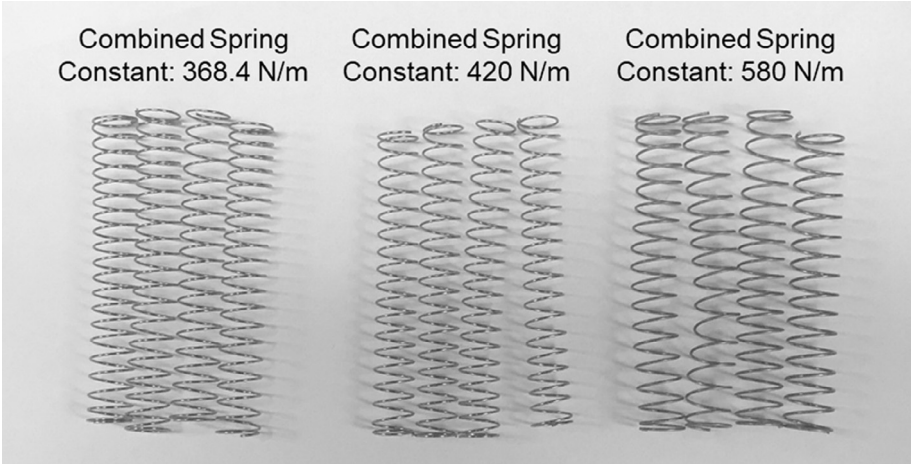

Fig. 28. Springs with different spring constants to simulate different suspension systems.

(a) DC1: Change of boundary conditions (b) DC2: Added mass at mid-span

Fig. 29. Damage applied to the bridge.

ing the voltage on Arduino board. The spring constant of the suspension system is changed by replacing the springs (see Fig. 28).

As shown in Fig. 29, two damage cases as well as baseline case are applied to the bridge:

1. DC1: Boundary condition change at both ends (Fig. 29(a)).
2. DC2: Added mass at mid-span (Fig. 29(b)).

In DC1, the boundary condition change is experimentally simulated by replacing rollers with short I-beams and connect the bridge deck to the short beam through four M12 bolts at each side. In DC2, two 5 kg steel blocks are softly attached to the bridge deck through clamps at mid-span.

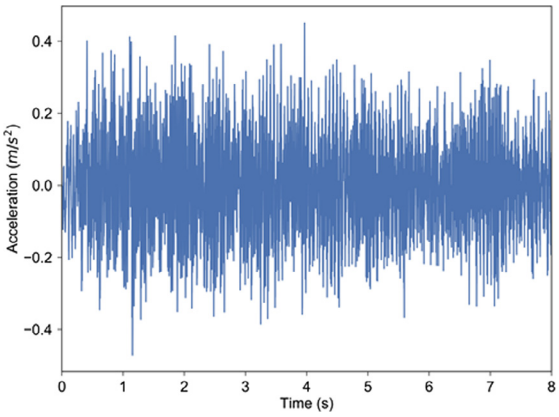

Fig. 30. Average acceleration taken from two PCB 393A03 accelerometers.

For each vehicle configuration, the test is repeated three times. Therefore, there are in total $3 \times 3 \times 3 \times 3 = 81$ tests for each damage case. Similar to numerical analysis, 60% of data in the healthy case are reserved for baseline, and 40% are for validation purpose.

Since the vehicle requires time to start and stop, the acceleration data near the ends are not reliable and are therefore truncated. The speed of the robot car is pre-set to the values in Table 1, but it is not precisely controlled by the program. This is to mimic the fact that vehicles on the bridge may not have constant speed. It should also be noted that only a single car is considered on the bridge at a time. The road roughness is not simulated explicitly in the experiments, but the existence of rust on the bridge deck is expected to simulate the road roughness.

4.2. Interpretation of results

Since there are two accelerometers installed on the car, the average of these two sensors is taken as input for our analysis to reduce the uneven movement of the top plate. Fig. 30 presents the average acceleration taken from the robot car with 2.350 kg top plate, 0.185 m/s speed, and 420 N/m spring constant passing over the baseline bridge. It should be noted that the first two seconds of the acceleration data is not used to avoid the disturbance of the engine startup.

Similar to numerical analysis, for different damage cases, the distributions of the transformed features extracted from MFC and PCA are shown in Fig. 31 in terms of boxplots. Regarding damage, DC1 is boundary condition change to simulate global damage, while DC2 is to put additional mass at mid-span to simulate local damage. Fig. 31(a) shows the distribution of transformed features for both baseline and validation data. Since both baseline and validation cases represent the same structural configuration (healthy), it is seen that all 6 transformed features have very similar distributions in terms of statistical characteristics such as median, quantiles and mean. However, the difference is not as small as in numerical analysis, this is because the experimental data are noiser and corrupted by other factors, such as vibration of the motors and road surface roughness. In Fig. 31(b), the distributions of transformed features for boundary condition change case (DC1) is compared with baseline case. It is seen that the difference between these distributions are much larger than in Fig. 31(a), which indicates the existence of structural change, i.e. damage. It should be noted that the variation for transformed features 1–4 is larger than for transformed features 5–6, which means transformed features 1–4 are more sensitive to the damage in this case. More detailed investigations about the sensitivity of transformed features to damage will be conducted in future. Fig. 31(c) shows the distributions of those transformed features for added mass case (DC2). The box plots for DC2 also deviate significantly from baseline case, but the difference is smaller than DC1, which indicates that DC2 is less severe than DC1.

As shown in Fig. 32, the DFs which are the Euclidean distances of the mean of transformed features as specified in Eq. (16) are calculated for both two damage cases. It is shown that DFs for both DC1 and DC2 are higher than validation case, which implies the existence of damage. In addition, DFs for DC1 is higher than DC2, which proves that boundary conditions change is more severe than putting additional mass locally. It should also be noted that the DFs are considered stable in the experiments when the data from vehicles are sampled differently even though the disparity among different samplings are higher than in numerical analysis.

5. Conclusions

This paper consists of two parts. In the first part, a novel damage feature derived from adapted MFCCs is developed for damage detection of bridges using drive-by data. To overcome the deficiencies from a single drive-by measurement, the concept of using mobile sensor network for structural health monitoring utilizing large amount of data is introduced in the second part. Under this framework, an improved version of the approach based on adapted MFCCs and PCA is proposed.

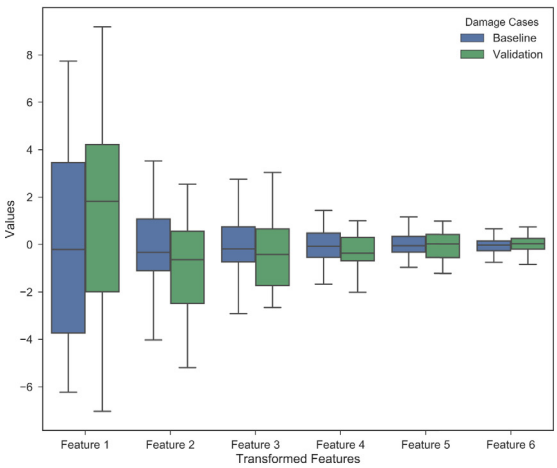

(a) baseline case and validation case

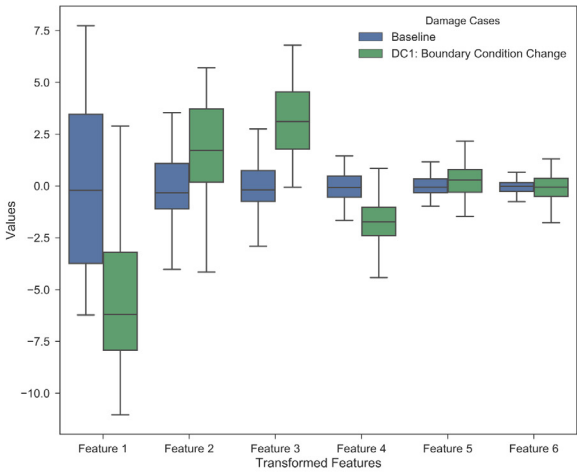

(b) baseline case and DC1

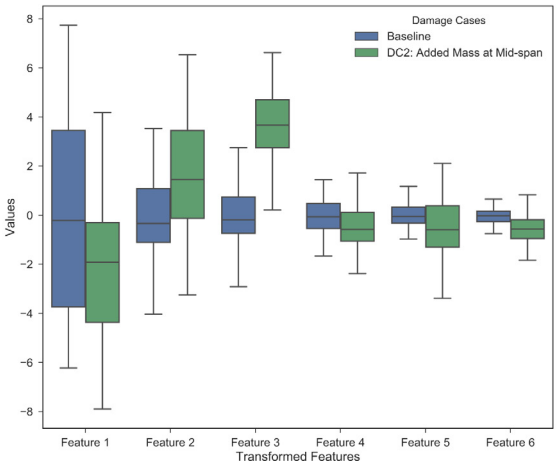

(c) baseline case and DC2

Fig. 31. Boxplot of transformed features for baseline case, validation case, DC1 and DC2.

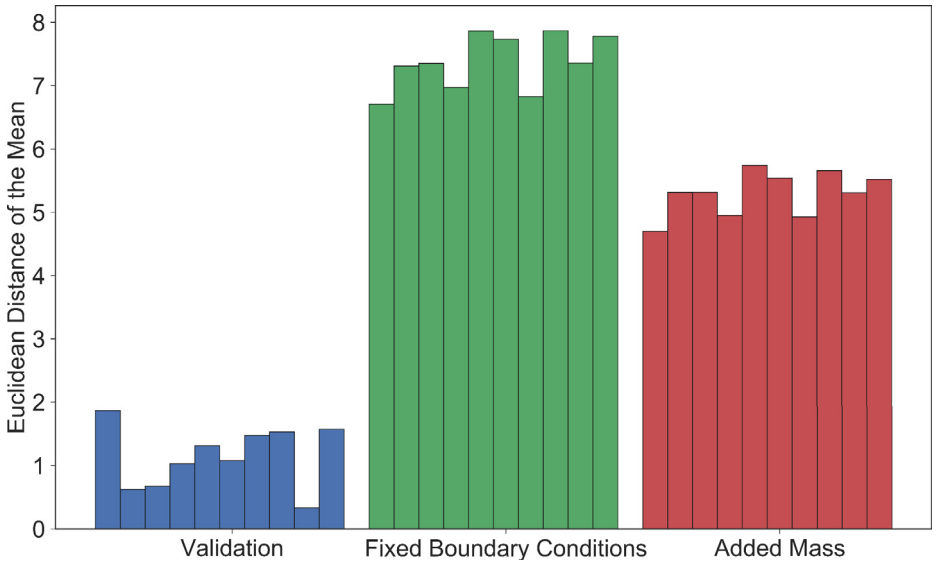

Fig. 32. DFs for different damage cases.

In this approach, the statistical characteristics of the transformed features from a large number of vehicles are extracted and compared. Both numerical analysis and experiments are conducted to verify the approach. To the best of the authors knowledge, this study is the first example exploring the feasibility of damage detection of bridges using drive-by measurement data from large number of vehicles numerically and experimentally. The following major conclusions are obtained from our analysis:

1. DFs based on MFCCs are very sensitive to the damage and robust to the noise. The damage, including stiffness change and boundary condition changes, can be successfully detected.
2. The values of DFs are related to the relative severity of the damage.
3. In the proposed approach, the damage can be detected and quantified using data from a large number of vehicles. No specific parameters from a single vehicle are required.
4. The potential of applying mobile sensor network for structural health monitoring is investigated. The research finds that usage of data from a large number of vehicular sensors for damage detection is feasible, and has the potential to monitor a population of bridges simultaneously and in almost real time.

In this paper, no attempts have been made to localize the damage using massive data from passing-by vehicles. In the future, the capability of the framework to localize damage will be investigated. In addition, this paper uses a relatively simple method to compare the statistical distributions of the features. More sophisticated techniques, like deep learning or time series analysis, will be investigated in future.

Acknowledgment

This research was supported by the Natural Sciences and Engineering Research Council of Canada through the Discovery Grants.

References

[1] H. Sohn, C.R. Farrar, F.M. Hemez, D.D. Shunk, D.W. Stinemates, B.R. Nadler, J.J. Czarnecki, A Review of Structural Health Monitoring Literature: 1996–2001, Los Alamos National Laboratory, 2003.
[2] C.R. Farrar, K. Worden, Structural Health Monitoring: A Machine Learning Perspective, John Wiley & Sons, Hoboken, 2012.
[3] Federal Highway Administration, Deficient Bridges by Highway System 2016, https://www.fhwa.dot.gov/bridge/nbi/no10/defbr16.cfm, 2016 (Nov 13, 2017).
[4] C. Soh, K.K. Tseng, S. Bhalla, A. Gupta, Performance of smart piezoceramic patches in health monitoring of a RC bridge, Smart Mater. Struct. 9 (2000) 533.
[5] J. Ko, Y. Ni, Technology developments in structural health monitoring of large-scale bridges, Eng. Struct. 27 (2005) 1715–1725.
[6] F.N. Catbas, M. Gul, J.L. Burkett, Conceptual damage-sensitive features for structural health monitoring: laboratory and field demonstrations, Mech. Syst. Sig. Process. 22 (2008) 1650–1669.
[7] M. Gul, F.N. Catbas, Statistical pattern recognition for structural health monitoring using time series modeling: theory and experimental verifications, Mech. Syst. Sig. Process. 23 (2009) 2192–2204.
[8] M. Chae, H. Yoo, J. Kim, M. Cho, Development of a wireless sensor network system for suspension bridge health monitoring, Autom. Constr. 21 (2012) 237–252.
[9] A. Khatir, M. Tehami, S. Khatir, I. Belaidi, S. Roger, M. Abdel Wahab, Damage detection and localization on thin plates using vibration analysis, 23rd International Congress on Sound and Vibration (ICSV23), International Institute of Acoustics and Vibration, 2016.
[10] Y.B. Yang, C.W. Lin, J.D. Yau, Extracting bridge frequencies from the dynamic response of a passing vehicle, J. Sound Vib. 272 (2004) 471–493.
[11] H.X. Hattori, F.N. He, H. Catbas, M. Furuta, Kawatani A bridge damage detection approach using vehicle-bridge interaction analysis and Neural Network technique, in: Bridge Maintenance, Safety, Management, Resilience and Sustainability, CRC Press, 2012, pp. 376–383.
[12] J. Kim, J.P. Lynch, Experimental analysis of vehicle–bridge interaction using a wireless monitoring system and a two-stage system identification technique, Mech. Syst. Sig. Process. 28 (2012) 3–19.
[13] Y. Zhang, S.T. Lie, Z. Xiang, Damage detection method based on operating deflection shape curvature extracted from dynamic response of a passing vehicle, Mech. Syst. Sig. Process. 35 (2013) 238–254.
[14] Z. Li, Damage Identification of Bridges from Signals Measured with a Moving Vehicle HKU Theses Online (HKUTO), The University of Hong Kong, Pokfulam, Hong Kong, 2014.
[15] J. Keenahan, E.J. OBrien, P.J. McGetrick, A. Gonzalez, The use of a dynamic truck–trailer drive-by system to monitor bridge damping, Struct. Health Monit. 13 (2014) 143–157.
[16] F. Cerda, S. Chen, J. Bielak, J.H. Garrett, P. Rizzo, J. Kovacevic, Indirect structural health monitoring of a simplified laboratory-scale bridge model, Smart Struct. Syst. 13 (2014) 849–868.
[17] X. He, M. Kawatani, T. Hayashikawa, C.-W. Kim, F.N. Catbas, H. Furuta, A structural damage detection approach using train-bridge interaction analysis and soft computing methods, Smart Struct. Syst. 13 (2014) 869–890.
[18] E.J. OBrien, A. Malekjafarian, A. González, Application of empirical mode decomposition to drive-by bridge damage detection, Eur. J. Mech.-A/Solids 61 (2017) 151–163.
[19] C.-W. Kim, K.-C. Chang, P.J. McGetrick, S. Inoue, S. Hasegawa, Utilizing moving vehicles as sensors for bridge condition screening—a laboratory verification, Sens. Mater. 29 (2017) 153–163.
[20] D. Hester, A. González, A discussion on the merits and limitations of using drive-by monitoring to detect localised damage in a bridge, Mech. Syst. Sig. Process. 90 (2017) 234–253.
[21] J. Bu, S. Law, X. Zhu, Innovative bridge condition assessment from dynamic response of a passing vehicle, J. Eng. Mech. 132 (2006) 1372–1379.
[22] Y. Zhang, L. Wang, Z. Xiang, Damage detection by mode shape squares extracted from a passing vehicle, J. Sound Vib. 331 (2012) 291–307.
[23] P.J. McGetrick, C.-W. Kim, A. González, E.J. Brien, Experimental validation of a drive-by stiffness identification method for bridge monitoring, Struct. Health Monit. 14 (2015) 317–331.
[24] T.J. Matarazzo, S.N. Pakzad, Structural identification for mobile sensing with missing observations, J. Eng. Mech. 142 (2016) 04016021.
[25] T.J. Matarazzo, S.N. Pakzad, Truncated physical model for dynamic sensor networks with applications in high-resolution mobile sensing and BIGDATA, J. Eng. Mech. 142 (2016) 04016019.

[26] A. Malekjafarian, P.J. McGetrick, E.J. OBrien, A review of indirect bridge monitoring using passing vehicles, Shock Vib. (2015 (2015)).
[27] D.G. Childers, D.P. Skinner, R.C. Kemerait, The cepstrum: A guide to processing, Proc. IEEE 65 (1977) 1428–1443.
[28] F. Zheng, G. Zhang, Z. Song, Comparison of different implementations of MFCC, J. Comput. Sci. Technol. 16 (2001) 582–589.
[29] W. Han, C.-F. Chan, C.-S. Choy, K.-P. Pun, An efficient MFCC extraction method in speech recognition, in: Proceedings. 2006 IEEE International Symposium on Circuits and Systems, 2006. ISCAS 2006, IEEE, 2006, p. 4.
[30] N. Dave, Feature extraction methods LPC, PLP and MFCC in speech recognition, Int. J. Adv. Res. Eng. Technol. 1 (2013) 1–4.
[31] N. Bochud, A.M. Gomez, G. Rus, J.L. Carmona, A.M. Peinado, Robust parametrization for non-destructive evaluation of composites using ultrasonic signals, in: 2011 IEEE International Conference on Acoustics, Speech and Signal Processing (ICASSP), IEEE, 2011, pp. 1789–1792.
[32] U. Dackermann, W.A. Smith, R.B. Randall, Damage identification based on response-only measurements using cepstrum analysis and artificial neural networks, Struct. Health Monit. 13 (2014) 430–444.
[33] G. Zhang, R.S. Harichandran, P. Ramuhalli, Application of noise cancelling and damage detection algorithms in NDE of concrete bridge decks using impact signals, J. Nondestr. Eval. 30 (2011) 259–272.
[34] L. Balsamo, R. Betti, H. Beigi, A structural health monitoring strategy using cepstral features, J. Sound Vib. 333 (2014) 4526–4542.
[35] D. O'shaughnessy, Speech Communication: Human and Machine, Universities press, 1987.
[36] T. Litman, Smart Transportation Investments II: Reevaluating The Role Of Public Transit For Improving Urban Transportation, (2006).
[37] A. Zanella, N. Bui, A. Castellani, L. Vangelista, M. Zorzi, Internet of things for smart cities, IEEE Internet Things J. 1 (2014) 22–32.
[38] T. Matarazzo, M. Vazifeh, S. Pakzad, P. Santi, C. Ratti, Smartphone data streams for bridge health monitoring, Procedia Eng. 199 (2017) 966–971.
[39] D.K. Harris, M. Alipour, S.T. Acton, L.R. Messeri, A. Vaccari, L.E. Barnes, The Citizen engineer: urban infrastructure monitoring via crowd-sourced data analytics, Struct. Congr. 2017 (2017) 495–510.
[40] A.-M. Yan, G. Kerschen, P. De Boe, J.-C. Golinval, Structural damage diagnosis under varying environmental conditions—part I: a linear analysis, Mech. Syst. Sig. Process. 19 (2005) 847–864.
[41] F. Magalhães, A. Cunha, E. Caetano, Vibration based structural health monitoring of an arch bridge: from automated OMA to damage detection, Mech. Syst. Sig. Process. 28 (2012) 212–228.
[42] D. Garcia, R. Palazzetti, I. Trendafilova, C. Fiorini, A. Zucchelli, Vibration-based delamination diagnosis and modelling for composite laminate plates, Compos. Struct. 130 (2015) 155–162.
[43] C. Zang, M. Imregun, Structural damage detection using artificial neural networks and measured FRF data reduced via principal component projection, J. Sound Vib. 242 (2001) 813–827.
[44] D. Tibaduiza, L. Mujica, J. Rodellar, Damage classification in structural health monitoring using principal component analysis and self-organizing maps, Struct. Control Health Monit. 20 (2013) 1303–1316.
[45] S. Park, J.-J. Lee, C.-B. Yun, D.J. Inman, Electro-mechanical impedance-based wireless structural health monitoring using PCA-data compression and k-means clustering algorithms, J. Intell. Mater. Syst. Struct. 19 (2008) 509–520.
[46] I.T. Jolliffe, in: Principal Component Analysis and Factor Analysis, Principal Component Analysis, Springer, 1986, pp. 115–128.